Influencing the Optoelectronic Properties of a Heteroleptic Iridium Complex by Second-Sphere H-Bonding Interactions

Barbora Balónová,[†,‡] Diego Rota Martir,[§] Ewan R. Clark,[‡] Helena J. Shepherd,[‡]
Eli Zysman-Colman,*[,§] Barry A. Blight*[,†,‡]

†University of New Brunswick, Department of Chemistry, Fredericton, NB, Canada, E3B 5A3

‡School of Physical Sciences, University of Kent, Canterbury, UK, CT2 7NH

§Organic Semiconductor Centre, EaStCHEM School of Chemistry, University of St Andrews, St Andrews, Fife, UK, KY16 9ST

ABSTRACT. The use of a new second-sphere coordination methodology for emission color tuning of iridium complexes is presented. We demonstrate that a complimentary H-bonding guest molecule binding through contiguous triple H-bonding interactions can induce a shift in the emission of the iridium complex from green to blue without the need to alter the ligand structure around the metal centre, while simultaneously increasing the photoluminescence quantum yield in solution. The association constant for this host-guest interaction was determined to be $K_a = 4.3 \times 10^3$ M^{-1} in a solution of 2% dimethylsulfoxide in chloroform by UV-Vis titration analysis and the impact of the hydrogen bonding interaction further probed by photoluminescence,

electrochemical, and computational methods. Our findings suggest that directed self-assemblies are an effective approach to influencing emission properties of phosphorescent iridium (III) complexes.

INTRODUCTION

Cyclometalated Ir[III] complexes are under intense investigation due to their high photoluminescence (PL) efficiency, relatively short PL lifetimes and wide range of accessible colors across the visible spectrum.[1] These complexes have been used in myriad applications such as biological labelling agents,[2] oxygen sensors,[3] photocatalysts for hydrogen production,[4] and as emitters in electroluminescent devices.[5] Notably, color tuning of these complexes is typically achieved through the modification or functional group substitution of ancillary and/or cyclometalating ligands.[6] There have been no reports in which second-sphere coordination, and in particular H-bonding, is cited as a viable methodology in tuning the electronic properties of these complexes. Until recently, hydrogen bonding in iridium complexes have been limited to H-bonds aimed at structure retention for biomimetic organo- and photocatalysis.[7] Lu and coworkers have reported an Ir-centered picolinate structure that uses peptidic interactions to assemble a luminescent donor-acceptor system.[8] This host-guest macrostructure, with pendant H-bonding moieties that are branched from the picolinate ligand, showed both promising photo- and electroluminescent behavior. The authors did not, however, quantify the strength of the intermolecular interactions.

Our work takes inspiration from a novel quadruple H-bonded heterodimeric assembly first reported by Leigh and co-workers, in which a protonated guanidinium species provided two

stabilizing features for the assembly process: 1) ion-dipole interaction between the H-bond-rich cationic guest and the annulated tetraazatetracene host; 2) reduction of destabilizing rotational isomerization using intramolecular H-bonding of the guanidinium with an adjacent benzimidazole.[9] We now posit that cyclometalation (of the N^N⁻ variety) in place of protonation would satisfy these two stabilization parameters while accessing additional physical properties imparted by the chosen transition metal; in the case of iridium(III), would generate charge neutral complexes.

In this account, we present an alternative route for tuning the emission properties of Ir^{III} complexes via direct second-sphere coordination.[10] Specifically, triple H-bonded heterodimeric system (**1•3**) exhibits modulated photophysical properties from that of the corresponding mononuclear cyclometalated Ir^{III} complex **1** (Figure 1). This work represents a first example of chromophoric units assembled into a higher-order structures via H-bonding, formed from a neutral N^N guanidine-chelated iridium (III) complex. This methodology can be easily extended towards the development of multinuclear assemblies incorporating tunable PL properties.
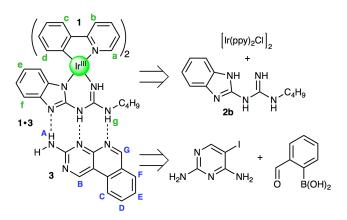

Figure 1. Host guest complex **1•3** is presented with a limited retrosynthetic analysis of each component.

EXPERIMENTAL SECTION

Materials. All starting materials were purchased from commercial sources and used without further purification. Analytical thin layer chromatography was done on precoated TLC sheets Alugram Sil G/UV254. Column chromatographic purifications were done with silica gel, ultra-pure, 60-200 micrometer (60 Å) or aluminum oxide (activated, neutral) as specified. All experiments were performed under a dry N_2 atmosphere using standard Schlenk techniques unless otherwise noted. All materials were used in the condition as received from the supplier without further purification unless otherwise noted.

NMR. ^1H (400 MHz) and ^{13}C (100 MHz) NMR spectra were recorded on a 'JEOL ECS 400' spectrometer in deuterated solvents such as chloroform-d, DMSO-d_6 or methanol-d_4 as noted. All chemical shifts are reported in δ (ppm) referenced to tetramethylsilane, $Si(CH_3)_4$, while peak multiplicities are referred to as singlet (s), doublet (d), triplet (t), quartet (q), broad singlet (bs), and multiplet (m).

Mass Spectrometry, Infrared, Elemental and Melting Point Analyses. High-resolution mass spectral data were recorded on Bruker MicrOTOF-Q II Instrument. IR spectra were recorded using Shimadzu IRAffinity-1 spectrophotometer. Elemental analysis was performed by the Elemental Analysis Service at the London Metropolitan University, UK. Melting points were determined on Buchi Melting Point Instrument.

UV-Visible Absorption. Absorption spectra were recorded at room temperature using Shimadzu UV-1800 double beam spectrophotometer. Molar absorptivity determination was verified by linear least-squares fit of values obtained from at least four independent solutions at varying concentrations with absorbance ranging from 2.8 x 10^{-4} to 2.4 x 10^{-5} M.

Photoluminescence Analyses. Steady-state emission and excitation spectra and time-resolved emission spectra were recorded at 298 K using an Edinburgh Instruments F980. All samples for steady-state measurements were excited at 360 nm and the samples for time-resolved measurements at 378 nm using a PDL 800-D pulsed diode laser. Photoluminescence quantum yields (PLQY) were determined using the optically dilute method,[11] using quinine sulfate as a reference (54.6%; 0.5 M H_2SO_4).[12]The PLQY of each component and the co-complex are the average values measured in triplicate and the estimated error is 5%. Photoluminescence quantum yield measurements of thin films were performed in an integrating sphere under a nitrogen purge in a Hamamatsu C9920-02 luminescence measurement system.[13] Further details of all PL analyses are available in the supporting information (See SI, Section 5).

Electrochemistry. Cyclic voltammetry (CV) measurements were performed in an Innovative Technology glovebox using a standard three electrode system connected to a Biologic SP-150 potentiostat. Solutions for CV were prepared in DCM solution with 0.1M of tetrabutylammonium hexfluorophosphate ($TBAPF_6$) as the electrolyte at 298 K. The cells consisted of a platinum disk working electrode (0.07 cm^2), a platinum wire counter electrode, and a Ag/Ag^+ reference electrode. Concentration of active species: 2mM, potential range 0–2.2 V, scan rate 100 mV s^{-1}. Recrystallized ferrocene was used as the internal standard and all potentials are reported vs SCE [14] using the formal potential of ferrocene / ferrocenium in DCM, which is 0.46 V vs SCE[14] in 0.1 m $TBAPF_6$ solution.

Single Crystal X-ray Diffraction. $C_{35}H_{33}Cl_3IrN_7$ (M =850.23 g/mol): triclinic, space group P-1 (no. 2), $a = 14.4927(8)$ Å, $b = 15.4171(11)$ Å, $c = 17.5785(11)$ Å, $\alpha = 103.021(6)°$, $\beta = 103.260(5)°$, $\gamma = 112.155(6)°$, $V = 3322.1(4)$ Å^3, $Z = 4$, $T = 100.00(10)$ K, $\mu(MoK\alpha) = 4.298$ mm^{-1}, $Dcalc$c= 1.700 g/cm^3, 58513 reflections measured ($4.584° \leq 2\Theta \leq 59.302°$), 16652 unique ($R_{int} = 0.0993$,

R$_{sigma}$ = 0.1330) which were used in all calculations. The final R_1 was 0.0623 (I > 2σ(I)) and wR_2 was 0.1110 (all data). Suitable crystals were grown by slow vapour diffusion of hexanes into a solution of **1** dissolved in CHCl$_3$ and mounted on a Rigaku Oxford Diffraction Supernova diffractometer. The data was refined by least squares minimization using ShelXL[15] and solved by intrinsic phasing using ShelXT. [16] Olex2 [17] was used as an interface to all ShelX programs. Hydrogen atoms located on N6, N13, N5 and N12 could not be located from the difference map. To ensure a chemically sensible model, hydrogen atoms were modelled at calculated positions for all four possible locations, and occupancy was fixed at 50% in all cases. The butyl chain on one of the two independent molecules is disordered, along with one molecule of chloroform over two positions, each with 50% occupancy. CCDC 1822594 contains the supplemental crystallographic information and is available free of charge from the Cambridge Crystallographic Database.

Host-Guest Titrations. All dilutions and titrations were performed using Hamilton Gastight microliter syringes at room temperature. NMR dilution studies of complex **1** (5x10^{-3} M) were performed in CD$_2$Cl$_2$ with addition of appropriate aliquots of CD$_2$Cl$_2$. UV-Vis dilution studies of complex **1** (6x10^{-5} M) were performed in HPLC grade dichloromethane with addition of appropriate aliquots of HPLC grade dichloromethane. UV-Vis titration studies were performed with host **1** (1 x10^{-5} M) and titrated with the addition of appropriate aliquots of a solution of guest **3** (1 x 10^{-4} M) with a background concentration of host (1 x10^{-5} M) to maintain a constant concentration of host throughout the study. All dilution and titration data were analyzed with the program BindFit [18,19].

Synthesis. 1-(1_H_-benzo[_d_]imidazol-2-yl)-3-butylthiourea 2a. Compound **2a** is known [20] but was synthesized using an alternative modified procedure.[21] To a solution of _N_-(benzoimidazol-2-yl)-imidazole-1-carbothioamide (0.46 g, 1.9 mmol) in DMF (20 mL) was added 0.1 equiv. of 4-

6

N,N-dimethylaminopyridine followed by dropwise addition of *n*-butyl amine (0.19 mL, 1.9 mmol) while stirring. The reaction mixture was stirred at 100 °C for 15 h. After cooling down to r.t. the reaction mixture was poured into ice-cold water and stirred for 1 h. A white-milky color precipitate was filtered and was washed with water (2 x 15 mL) and further purified by column chromatography (EtOAc / hexane, 3:2. R_f = 0.2). Fractions were collected and the solvent removed by rotary evaporation. The product **2a** was dried in a vacuum oven at 40 °C overnight. Pale yellow title compound was obtained in 70% yield. ^{1}H NMR (400 MHz, 298 K, DMSO-d_6): δ 11.13 (t, 3H, J = 58.7 Hz), 7.44 (s, 2H), 7.19 – 7.04 (m, 2H), 3.64 (d, 2H, J = 5.8 Hz), 1.69 – 1.53 (m, 2H), 1.46 – 1.32 (m, 2H), 0.92 (dt, 3H, J = 19.3, 6.7 Hz). ^{13}C NMR (100 MHz, 298 K, DMSO-d_6): δ 177.82, 148.19, 140.39, 131.32, 121.78, 116.91, 111.45, 44.36, 39.52, 30.59, 19.94, 13.92. M.p. 147-150 °C. EI-MS *m/z calculated:* 247.10 *found:* 248.11 [M+]. Anal. calcd. for $C_{12}H_{16}N_4S$: C, 58.04; H, 6.49; N, 22.56. Found: C, 57.93; H, 6.54; N, 22.40.

1-(1*H*-benzo[*d*]imidazole-2-yl)-3-butylguanidine 2b. From a modified procedure,[22] compound **2a** (269 mg, 1.08 mmol) was suspended in 15 mL of $CHCl_3$ and to this were added HgO (0.32 g, 1.51 mmol) and 2 M methanolic NH_3 (6 mL). The reaction mixture was stirred at r.t. for 3 h and a color change from wine red to brown was observed. The reaction was then filtered through celite and concentrated under reduced pressure. The resulting solid was dissolved in 2 M acetic acid (~ 8 mL) and stirred for 1 h, then filtered through celite. The pH was adjusted to 8.0 by addition of a 10 M solution of NaOH. The formed precipitate was filtered, washed with water and dried. The product was dissolved in chloroform and extracted 3 x with saturated solution of $NaHCO_3$. The organic phase was separated and dried over $MgSO_4$ and the solvent removed under reduced pressure. The final product was dried overnight in a vacuum oven at 40 °C. Title compound **2b** was obtained as white powder in 50% yield. ^{1}H NMR (400 MHz, 298 K, DMSO-

d_6): δ 11.00 (s, 1H), 7.20 (d, 1H, $J = 7.3$ Hz), 7.07 (d, 1H, $J = 7.1$ Hz), 6.98 – 6.78 (m, 2H), 3.21 (dd, 2H, $J = 12.7, 6.9$ Hz), 1.48 (dd, 2H, $J = 14.8, 7.3$ Hz), 1.36 (dt, 2H, $J = 14.7, 7.2$ Hz), 0.92 (t, 3H, $J = 7.3$ Hz). ^{13}C NMR (100 MHz, 298K, DMSO-d_6): δ 159.05, 157.66, 142.59, 132.21, 119.65, 118.99, 114.94, 108.48, 40.07, 39.52, 31.49, 19.66, 13.80. M.p. 190-208 °C. EI-MS m/z *calculated:* 231.15 *found:* 232.16 [M+]. Anal. calcd. for $C_{12}H_{17}N_5$: C, 62.31; H, 7.41; N, 30.28. Found: C, 62.12; H, 7.55; N, 30.06.

Iridium Complex 1. The iridium dimer complex **[Ir(ppy)₂Cl]₂** (39.7 mg, 3.70 x10^{-5} mol),[23] guanidine **2b** (13.2 mg, 2.5 equiv.) and potassium carbonate (50 mg, 10 equiv.) were added to 12 mL of dry toluene. The reaction mixture was stirred overnight at 110 °C under a N₂ atmosphere. The solvent was removed under reduced pressure. A small amount of dichloromethane was added to dissolve the solid (8 - 12 mL) and the mixture was extracted with water (3 x 20 mL) to remove the excess base. The organic layers were combined and the solvent removed under reduced pressure. Further purification included precipitation and column chromatography (silica gel, DCM/MeOH, 10:0.25 - 10:1, $R_f = 0.3$). Final product **1** was obtained as a bright yellow powder in 44% yield. ^{1}H NMR (600 MHz, 298 K, chloroform-d): δ 8.68 (dd, 1H, $J = 5.9, 0.8$ Hz), 8.15 – 8.04 (m, 1H), 7.88 (d, 1H, $J = 8.1$ Hz), 7.78 (d, 1H, $J = 8.0$ Hz), 7.73 (td, 1H, $J = 8.0, 1.6$ Hz), 7.67 (dd, 1H, $J = 7.4, 1.3$ Hz), 7.60 (d, 2H, $J = 7.8$ Hz), 7.15 (d, 1H, $J = 7.9$ Hz), 7.08 (ddd, 1H, $J = 7.3$, 5.9, 1.3 Hz), 7.01 – 6.87 (m, 4H), 6.79 (dtd, 2H, $J = 20.6, 7.4, 1.3$ Hz), 6.68 – 6.62 (m, 1H), 6.43 (dd, 1H, $J = 7.6, 0.8$ Hz), 6.24 – 6.19 (m, 1H), 6.15 (s, 1H), 6.09 (d, 1H, $J = 8.3$ Hz), 5.72 (s, 1H), 4.56 (s, 1H), 3.04 – 2.78 (m, 2H), 1.41 (ddd, 2H, $J = 14.0, 7.1, 3.5$ Hz), 1.23 (dd, 2H, $J = 14.0, 6.6$ Hz), 0.79 (t, 3H, $J = 7.3$ Hz). ^{13}C NMR (100 MHz, 298K, chloroform-d): δ 169.15, 168.17, 153.61, 151.88, 151.57, 150.01, 148.83, 147.52, 144.62, 144.47, 141.20, 136.82, 136.51, 133.05, 132.01, 129.72, 124.57, 124.01, 122.63, 121.84, 121.62, 121.33, 121.08, 118.80, 116.86, 110.65, 77.16,

41.06, 30.85, 20.05, 13.76. EI-MS *m/z calculated:* 731.2348 *found:* 732.2450 [M+]. Anal. calcd. for $C_{34}H_{32}IrN_7$: C, 55.87; H, 4.41; N, 13.41. Found: C, 55.96; H, 4.31; N, 13.35.

Pyrimido-[4,5-*c*]isoquinolin-3-amine 3. 5-iodopyrimidine-2,4-diamine (197 mg, 8.34×10^{-4} mol), 2-formylphenyl boronic acid (182 mg, 1.21 mmol), potassium carbonate (0.461 g, 3.33 mmol) and tetrakis(triphenylphosphine)palladium(0) (1.4 mg, 0.5 mol%) were added to the mixture of dioxane and water (3:1, 9 mL of dioxane, 3 mL of water). The reaction mixture was heated under reflux for 3 h, then cooled to r.t. and placed in cold bath. The precipitate filtered and washed with water (2 x 30 mL), three times suspended and sonicated in water and filtered, then finally dried in a vacuum oven (24 h, 40 °C). Product **3** (82 mg) was obtained as a fine bright yellow powder in 50% yield. ^{1}H NMR (400 MHz, 298K, DMSO-d_6): δ 9.88 (s, 1H), 9.50 (s, 1H), 8.72 (d, 1H, *J* = 8.1 Hz), 8.17 (d, 1H, *J* = 7.5 Hz), 7.92 (ddd, 1H, *J* = 8.4, 7.3, 1.3 Hz), 7.70 – 7.63 (m, 1H), 7.18 (s, 2H). ^{13}C NMR (100 MHz, 298 K, DMSO-d_6): δ 163.68, 161.43, 158.80, 158.50, 132.58, 132.22, 129.33, 126.43, 124.43, 124.41, 120.35, 107.00. EI-MS *m/z calculated:* 196.07 *found:* 197.08 [M+]. M.p. > 280 °C. Anal. calcd. for $C_{11}H_8N_4$: C, 67.34; H, 4.11; N, 28.55. Found: C, 67.19; H, 4.25; N, 28.35.

RESULTS AND DISCUSSION

Complex **1** was synthesized by refluxing benzimidazolyl-guanidine **2b** with the iridium μ-chloro-bridged dimer [Ir(ppy)$_2$Cl]$_2$ (ppyH = 2-phenylpyrdine)[23] in the presence of an excess of base in toluene. Isolation, after purification by column chromatography, yielded **1** as a yellow solid. Compound **3** was prepared by reacting 2, 4-diamino-5-iodopyrimidine [24] with 2-formylphenylboronic acid, following a modified tandem Suzuki-Miyaura cross-coupling / imine condensation / cyclization procedure.[25]

Single crystals of **1** suitable for X-ray diffraction study were obtained by slow vapour diffusion of hexanes into a chloroform solution of **1**. Complex **1** crystallized in the triclinic space group P-1 as a H-bonded dimer (Figure 2). As expected, the central iridium atoms of the dimer are bonded to two ppy ligands via bidentate C^N ligation with the nitrogen atoms in a mutually *trans* configuration, and to the guanidine benzimidazolate ligand **2b** as a 6-membered N^N⁻ chelate. Of interest to us are the observed intermolecular N5···N12 and N6···N13 contact distances (a=2.76 Å, b =2.91 Å), which are less than the sum of van der Waals radii (characteristic for this type of interaction), and an affirmation of our approach. [26] Given this result in the solid-state, we proceeded to quantify this interaction in solution using both UV-Vis absorption and ^{1}H NMR dilution experiments.
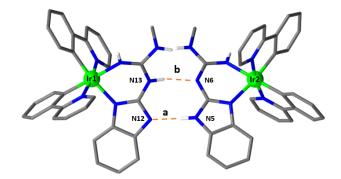

Figure 2. X-ray crystal structure of complex **1** with annotated NH…N contacts (orange); a) N5···N12 = 2.76 Å, NH···N = 158°; b) N6···N12 = 2.91 Å, NH···N = 161°. All CH-hydrogens and butyl chain are omitted for clarity.

The overall dimerization constant was determined by UV-Vis absorption studies to be K_d = 25 M^{-1} in dichloromethane (DCM; see SI Section 3, Figure S8), which was confirmed by ^{1}H NMR in CD$_2$Cl$_2$ (K_d=23 M^{-1}).[18] This suggests that a high concentration, on the order of 10^{-2} M, is required for **1** to homodimerize in DCM, and thus a minimal destructive energy is sufficient to

disassemble the dimer in DCM to form the proposed triple H-bonding heterodimeric system **1•3** (Figure 1). It was expected that **1•3** would form a stronger interaction than the homodimer structure of **1**, which is merely comprised of two alternating H-bonds. Indeed, the enthalpy gained in introducing additional interactions can influence the complexation strength in **1•3**, particularly when the effects of secondary attractive and/or repulsive interactions are considered. Adduct **1•3** can be described by a H-bond donor (D) and acceptor (A) arrangement comprising of a contiguous AAD-DDA array. The strength of the association of this heterodimeric system was assessed by UV-Vis absorption titration of **1** with **3** (CHCl$_3$/DMSO 98:2), revealing an association constant of K$_a$ = 4.3 x 10^3 M^{-1} (See SI, Section S3, Figure S9).[18] A comparison of ^{1}H NMR stacked spectra is presented in Figure 3. Dashed lines show shifts upon formation of complex **1•3**.
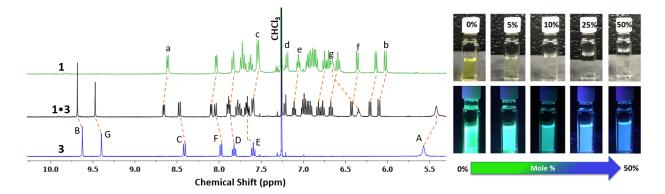

Figure 3. Left: ^{1}H NMR (400 MHz, 1 x 10^{-3} M, CDCl$_3$, 298 K) comparison in chloroform-*d*: compound **1** (green); complex **1•3**; (black); compound **3** (blue). Right: Demonstration of chromaticity shift with increasing mole percentage of **3** to a DCM solution of **1** under ambient and UV (365 nm) light.

A comprehensive photophysical study of assembly **1•3** and its individual components was undertaken in DCM solution and as 5 wt% polymethylmetacrylate (PMMA) doped films (Figure 4a). The UV-vis absorption spectra of **1** and **1•3** in DCM (see SI, Section S5, Figure S11) show intense bands at 250 – 300 nm that are assigned to the spin-allowed π-π* transitions. The weaker

bands at wavelengths longer than 320 nm result from both singlet and triplet metal-to-ligand (Ir(dπ) to C^N) and ligand-to-ligand (N^N to C^N) charge transfer (^{1}MLCT/LLCT) transitions and the complex shows comparable behavior to other neutral iridium complexes containing two ppy C^N ligands.[27] The photophysical properties of **1**, **1•3** and **3** are summarized in Table 1 and their emission spectra are illustrated in Figures 4a and 4b. Complex **1** is a green emitter with a λ_{PL} at 491 nm and a shoulder peak at 518 nm (Φ_{PL} = 20%), indicative of an emission from a ligand-centered state. The mono-exponential emission lifetime (τ_{PL}) of 0.70 μs observed for **1** (λ_{ex} = 378 nm) indicates the presence of a single emissive species. The emission of **1** in the PMMA-doped film is modestly bathochromically shifted to 498 nm and the Φ_{PL} of **1** is enhanced in the solid state to 34%.

With the introduction of the complement **3**, we observed a modest increase of the overall Φ_{PL} for adduct **1•3** in DCM (Φ_{PL} = 25%) compared to free component **1** (Φ_{PL} = 20%) along with a color change from green (λ_{PL} = 491, 518 nm) to deep blue (λ_{PL} = 425, 494 nm) (CIE diagram of **1**: x= 0.23, y=0.56; **1•3**: x=0.18, y=0.20; see SI, Section S5, Figure S28).[28] Dual emission is observed, primarily ascribed to the components themselves, which is coupled with energy transfer from **3** to **1** as evidenced by the altered bi-exponential decay of τ_{PL} = 0.75 and 0.33 μs (λ_{ex} = 378 nm and collected at λ_{em} = 500 nm) in comparison to the emission decays of **1** and **3** (0.70 μs at λ_{em} = 500 nm and 3.0 ns at λ_{em} = 400 nm, respectively). It is important to note that at 378 nm both components are directly photoexcited. We nevertheless ascribe the longer lifetime component to the direct photoexcitation of **1** (93% contribution), which is slightly elongated from that of free **1**. We rationalize this small increase to be caused by an electronic perturbation of **1** imparted by the formation of host-guest complex **1•3**. The shorter component can be linked to the excitation of **3** (7% contribution), and subsequent energy transfer to **1** in **1•3**. We see no evidence of the lifetime

component of free **3**.[29] We also collected the decay lifetime of **1•3** at λ_{em} = 450 nm where both species exhibit photon emission. At this emission wavelength, the luminescence decay is dominated by the phosphorescence of **1** (τ_{PL} = 0.60 µs; 95% contribution; see SI, Section 5, Figure S26) with a minor contribution from fluorescent **3** (τ_{PL} = 2.7 ns), demonstrating that the lifetime values are λ_{em} dependent and attributed to a bimolecular system with coupled emission properties. This conclusion is further supported by comparison of the emission spectra of **1**, **3** and **1•3** at equimolar concentrations (see Figure 4b), where some emission quenching is evident of both components.

This phenomenon was also explored by performing a PL titration experiment (see SI, Section 5, Figure S19) of **1** titrated with **3** (with a background concentration of **1** to maintain a constant concentration) in CHCl$_3$/DMSO 98:2, modelling the same conditions as the UV-Vis binding study. Here, we see an increase of the emission intensity of **3** up to the equimolar mark with some quenching of **1** observed. Beyond a 1:1 concentration, we observe little increase (followed by some quenching) in emission intensity of **3** upon addition of up to 4 equivalents of **1**, while only a partial quenching of **1** was observed. This experiment clearly illustrates that the emission properties of this host-guest pair are coupled. The energy transfer efficiency for **1•3** was also measured and calculated to be approximately 35% from the ratio between the corrected excitation spectrum of **1•3** (collected at 580 nm; beyond the emission window of **3**) and the absorption spectrum of **1•3** (Figure 4c).
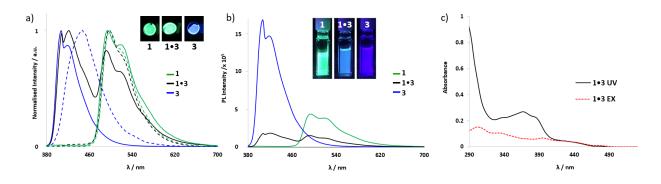
Figure 4. a) Normalized emission spectra of solution (DCM at 5 x 10^{-5} M; solid lines) and solid state (PMMA films; dashed lines) of **1** (green), **3** (blue) and **1•3** (black); inset: photos of PMMA films deposited on quartz slides (λ_{ex} = 360 nm). b) Non-normalized emission spectra in DCM (5 x 10^{-5} M) illustrating quenching phenomenon with addition of **3** to **1**; inset: photos of DCM solution in quartz cuvettes. c) Absorption (solid black line) and corrected PL excitation (red dashed line; measured at 580 nm) spectra normalized to absorbance at 430 nm.

The Φ_{PL} for the PMMA doped film prepared in 1:1 ratio of **1** and **3** to form **1•3** adduct is 23% (Table 1), with near quantitative quenching of **3**. To probe the emission quenching of **3**, a PMMA doped film containing a 1:1 ratio of **3** and the yellow emitting [Ir(ppy)$_2$(dtbubpy)]PF$_6$ (dtbubpy is 4,4'-di-*tert*-butyl-2,2'-bipyridine),[30] was prepared and analyzed. Here, no association by hydrogen bonding is present between both emitting species but, similarly to **1•3**, we observed a complete emission quenching of **3**. This demonstrates that one root cause of the quenching of **3** in both cases is due to aggregation-caused quenching in doped film. This is supported by an analogous experiment conducted in solution demonstrating that the emission of **3** was also quenched in solution but to a lesser extent, while ^{1}H NMR analysis shows no discernable interactions with [Ir(ppy)$_2$(dtbubpy)]PF$_6$ (See SI, Section S5, Figures S15-18). The reduced loss of signal in the solution PL study also demonstrates that we are perturbing the [Ir(ppy)$_2$(dtbubpy)]PF$_6$ signal less than that of **1•3**. This indicates that the intermolecular

interactions afforded by the recognition motif in **1•3** are influencing the energy transfer (ET) in solution, the efficiency of which is a function of the distance between the donor and the acceptor units.[31] This does not rule out, however, quantitative ET from **3** to **1** in the solid-state since the quantum yields of **1•3** decrease slightly compared to solution data, while the opposite is true for **1**. Given the highly conjugated nature of **3**, its propensity to potentially act as an electron-transport/host material is also a likely contributor to this observation, and an avenue we are investigating further in the context of EL devices.

Electrochemical studies on complex **1**, assembly **1•3**, and compound **3** were performed using cyclic voltammetry (CV) and potentials of interest (vs. SCE)[14] reported in Table 1; CV traces are included in the SI (see Section S6, Figure S30). Complex **1** exhibits a oxidation at E_{pa}= 1.12 V, assigned to the Ir (III)/Ir (IV) redox couple[32] with contributions from the N^N⁻ ligand. Upon introduction of **3** to a solution of **1**, the potential of adduct **1•3** is anodically shifted to 1.17 V due to the formation of **1•3** H-bonded complex, which act to remove electron density from the benzimidazole portion of the N^N⁻ ligand (the H-bond acceptor with the highest density of HOMO occupancy), thereby stabilizing the complex.[33] This analysis is further supported by the DFT calculations where the T_1 spin-density distributions show spin density shared across both components of **1•3** (Figure 5). This intermolecular electronic communication between the heterodimer is further corroborated by DFT calculations where the frontier HOMO orbitals are situated largely on the Ir^{III} centre and the N^N⁻ ligand while the LUMO is entirely localized on **3**. Thus, in both the ground and the excited states there is an electronic coupling between **1** and **3** in **1•3**. Finally, the thermal stability was investigated by thermogravimetric analysis (TGA) under a nitrogen atmosphere. Complex **1** is thermally stable with a 5% weight-decomposition temperature T_d = 288 °C, which is desirable for possible implementation into OLED devices.
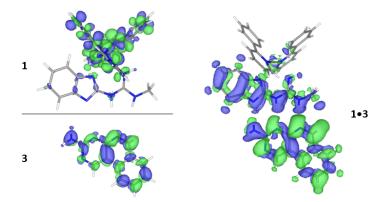
Figure 5. Geometry optimized triplet spin-density difference distributions of **1**, **3**, and **1•3**; B3LYP/LANL2DZ & 6-311G (d,p) basis sets.

Table 1. Photophysical and electrochemical data for complexes **1**, **3** and **1•3**.[a]

Complex	λ_{PL}/ nm	CIE / x,y	τ_{PL}[b] / µs	Φ_{PL}[c]	k_r[d]/ s^{-1}	k_{nr}[d]/ s^{-1}	E_{ox}[e]/ V
1	491,518	0.23,0.56	0.70	0.20	2.8×10^5	1.1×10^6	1.12
	(498,518)	(0.20, 0.59)	(0.4, 1.7)	(0.34)	(2.0×10^5)	(3.8×10^5)	
1•3	425,494	0.18,0.20	0.33, 0.75	0.25	3.3×10^5	1.3×10^6	1.17
	(497)	(0.19, 0.56)	(0.3, 1.6)	(0.23)	(1.4×10^5)	(4.8×10^5)	
3	409,426	0.15,0.03	3.0×10^{-3}	0.43	2.1×10^8	2.9×10^8	1.65
	(446)	(0.15, 0.08)	$(1 \times 10^{-3}, 4 \times 10^{-3})$	(0.07)	(1.6×10^7)	(2.3×10^8)	

[a]Solution data are reported in degassed DCM. Solid state data are represented in parentheses. Polymer doped films were prepared with 5% of emitter and 95% PMMA in 2-methoxyethanol and deposited by spin-coating on quartz substrate. **1•3** complex is 1:1 ratio of iridium complex **1** and compound **3**. All samples excited at 360 nm. [b]Emission lifetimes were collected by excitation at λ_{ex}= 378 nm. λ_{em} used to collect decay lifetimes are reported in the SI, Section 5, Fig. S20-S26. [c]Quinine sulfate employed as the external reference (Φ_{PL} = 54.6% in 0.5 M H$_2$SO$_4$ at 298 K).[12] [d] k_r and k_{nr} were calculated using the major lifetime component. [e] Measurements were carried out in DCM with 100 mV s^{-1} scan rate and data are reported vs. SCE in DCM.[13]

CONCLUSIONS

In summary, we have successfully demonstrated the design, synthesis, and characterization of a new heteroleptic cyclometalated iridium (III) complex using 2-phenylpyridinato C^N ligands and a benzimidazolate-linked guanidine ligand. The dimeric assembly of **1** exhibits green photoluminescence with emission maxima at 491 and 518 nm with 20% Φ_{PL} in DCM solution and 34% in 5 wt% PMMA doped film. We further demonstrated that **1** forms a host-guest assembly

with **3** in a complementary ADD-DAA H-bond arrangement with an association constant $K_a = 4.3$ x 10^3 M^{-1} (UV Vis, chloroform/DMSO, 98:2), resulting in a cumulative Φ_{PL} of 25%, with interactions further confirmed by ^1H NMR, PL analysis, CV, and computational analysis. Particularly noteworthy is that we see no evidence of proton-coupled electron transfer and few adverse effects when combining these electroactive H-bonding partners. This work clearly demonstrates that direct second-sphere coordination via H-bonding is a novel and effective methodology to alter photophysical properties of emitters, accessing a linear colour scale with a discretely interacting two component system, and in this case reaching into the deep-blue region by obviating the need for difficult synthetic manipulations of the ligand structure around the metal centre.

ASSOCIATED CONTENT

Supporting Information.

The Supporting Information (SI) is available free of charge on the ACS Publications website at DOI: 10.1021/xxxxxxx.

Experimental procedures, photophysical data, NMR, CV, computational studies, and supplementary XRD data (CCDC-1822594). (PDF)

AUTHOR INFORMATION

Corresponding Author

*B.Blight@unb.ca; Twitter: @DrBarryChem; *eli_journals@zysman-colman.com

ORCID

Notes

The authors declare no competing financial interests. The raw data which underpin this work are available at http://dx.doi.org/10.25545/YB60PU.

REFERENCES

(1) a) Lu, K.-Y.; Chou, H.-H.; Hsieh, C.-H.; Yang, Y.-H. O.; Tsai, H.-R.; Tsai, H.-Y.; Hsu, L.-C.; Chen, C.-Y.; Chen, I.-C.; Cheng, C.-H. Wide-Range Color Tuning of Iridium Biscarbene Complexes from Blue to Red by Different N∧N Ligands: An Alternative Route for Adjusting the Emission Colors. *Adv. Mater.* **2011**, *23*, 4933–4937. b) *Iridium (III) in Optoelectronic and Photonics Applications*, John Wiley & Sons, Ltd, **2017.**

(2) a) Kando, A.; Hisamatsu, Y.; Ohwada, H.; Itoh, T.; Moromizato, S.; Kohno, M.; Aoki, S. Photochemical Properties of Red-Emitting Tris(cyclometalated) Iridium(III) Complexes Having Basic and Nitro Groups and Application to pH Sensing and Photoinduced Cell Death. *Inorg. Chem.* **2015**, *54*, 5342–5357. b) Jiang, J.; Zhang, C.; Lin, W.; Liu, Y.; Liu, S.; Xu, Y.; Zhao, Q.; Huang, W. Long-Lived Phosphorescent Iridium (III) Complexes Conjugated with Cationic Polyfluorenes for Heparin Sensing and Cellular Imaging. *Macromol. Rapid Commun.* **2015**, *36*, 640–646.

(3) Medina-Rodriguez, S.; Denisov, S. A.; Cudre, Y.; Male, L.; Marin-Suarez, M.; Fernandez-Gutierrez, A.; Fernandez-Sanchez, J. F.; Tron, A.; Jonusauskas, G.; McClenaghan, N. D.; Baranoff, E. High Performance Optical Oxygen Sensors Based on Iridium Complexes Exhibiting Interchromophore Energy Shuttling. *Analyst* **2016**, *141*, 3090–3097.

(4) McDaniel, N. D.; Bernhard, S. Solar Fuels: Thermodynamics, Candidates, Tactics, and Figures of Merit. *Dalt. Trans.* **2010**, *39*, 10021–10030.

(5) a) Martir, D. R.; Momblona, C.; Pertegás, A.; Cordes, D. B.; Slawin, A. M. Z.; Bolink, H. J.; Zysman-Colman, E. Chiral Iridium(III) Complexes in Light-Emitting Electrochemical Cells: Exploring the Impact of Stereochemistry on the Photophysical Properties and Device Performances. *ACS Appl. Mater. Interfaces* **2016**, *8*, 33907–33915. b) Henwood, A. F.; Bansal, A. K.; Cordes, D. B.; Slawin, A. M. Z.; Samuel, I. D. W.; Zysman-Colman, E. Solubilized Bright Blue-Emitting Iridium Complexes for Solution Processed OLEDs. *J. Mater. Chem. C* **2016**, *4*, 3726–3737. c) Duan, J. P.; Sun, P. P.; Cheng, C. H. New Iridium Complexes as Highly Efficient Orange–Red Emitters in Organic Light-Emitting Diodes. *Adv. Mater.* **2003**, *15*, 224–228.

(6) a) Skórka, Ł.; Filapek, M.; Zur, L.; Małecki, J. G.; Pisarski, W.; Olejnik, M.; Danikiewicz, W.; Krompiec, S. Highly Phosphorescent Cyclometalated Iridium(III) Complexes for Optoelectronic Applications: Fine Tuning of the Emission Wavelength through Ancillary Ligands. *J. Phys. Chem. C* **2016**, *120*, 7284–7294. b) Henwood, A. F.; Zysman-Colman, E. Lessons Learned in Tuning the Optoelectronic Properties of Phosphorescent Iridium (III) Complexes. *Chem. Commun.* **2017**, *53*, 807– 826. c) Chau, N.-Y.; Ho, P.-Y.; Ho, C.-L.; Ma, D.; Wong, W.-Y. Color-Tunable Thiazole-Based iridium (III) Complexes: Synthesis, Characterization and Their OLED Applications. *J. Organomet. Chem.* **2017**, *829*, 92–100.

(7) a) Xu, W.; Arieno, M.; Löw, H.; Huang, K.; Xie, X.; Cruchter, T.; Ma, Q.; Xi, J.; Huang, B.; Wiest, O.; Gong, L.; Meggers, E. Metal-Templated Design: Enantioselective Hydrogen-Bond-Driven Catalysis Requiring Only Parts-per-Million Catalyst Loading. *J. Am. Chem. Soc*. **2016**, *138*, 8774–8780. b) Skubi, K. L.; Kidd, J. B.; Jung, H.; Guzei, I. A.; Baik, M.-H.; Yoon, T. P. Enantioselective Excited-State Photoreactions Controlled by a Chiral Hydrogen-Bonding Iridium Sensitizer. *J. Am. Chem. Soc*. **2017**, *139*, 17186–17192.

(8) Zhang, C.; Zeng, H.; Huang, Q.; Wang, Y.; Chai, Y.; Huang, Y.; Zhao, S.; Lu, Z. High-Performance Red Electrophosphorescent Devices Based on All-Solution-Processed Hydrogen-Bonded Supramolecular Material. *J. Mater. Chem. C* **2018**, *6*, 4095–4105.

(9) Blight B. A., Hunter C. A., Leigh D. A., McNab H., Thomson P. I. T. An AAAA–DDDD quadruple hydrogen-bond array. *Nat. Chem*., **2011**, *3*, 244-248.

(10) Sun, H.; Liu, S.; Lin, W.; Zhang, K. Y.; Lv, W.; Huang, X.; Huo, F.; Yang, H.; Jenkins, G.; Zhao, Q.; Huang, W. Smart Responsive Phosphorescent Materials for Data Recording and Security Protection. *Nat. Commun*. **2014**, *5*, 3601.

(11) Crosby, G. A.; Demas, J. N. The Measurement of Photoluminescence Quantum Yields. *J.Phys. Chem*. **1971**, *75*, 991-1024.

(12) Melhuish, W. H., Quantum Efficiencies of Fluorescence of Organic Substances: Effect of Solvent and Concentration of the Fluorescent Solute. *J. Phys. Chem*. **1961**, *65*, 229–235.

(13) Greenham, N. C.; Samuel, I. D. W.; Hayes, G. R.; Phillips, R. T.; Kessener, Y. A. R. R.;Moratti, S. C.; Holmes, A. B.; Friend, R. H., Measurement of absolute photoluminescence quantum efficiencies in conjugated polymers. *Chem. Phys. Lett*., **1995**, *241*, 89-96.

(14) Connelly, N. G.; Geiger, W. E. Chemical Redox Agents for Organometallic Chemistry.

Chem. Rev. **1996**, *96*, 877–910.

(15) Sheldrick, G. M. SHELXT: Integrated Space-Group and Crystal-Structure Determination. *Acta Crystallogr. Sect. A* **2015**, *71*, 3–8.

(16) Sheldrick, G. M. Crystal Structure Refinement with SHELXL. *Acta Crystallogr. Sect. C, Struct. Chem.* **2015**, *71* (Pt 1), 3–8.

(17) Dolomanov, O. V; Bourhis, L. J.; Gildea, R. J.; Howard, J. A. K.; Puschmann, H. OLEX2: A Complete Structure Solution, Refinement and Analysis Program. *J. Appl. Crystallogr.* **2009**, *42*, 339–341.

(18) www.supramolecular.org

(19) Thordarson, P. Determining Association Constants from Titration Experiments in Supramolecular Chemistry. *Chem. Soc. Rev.* **2011**, *40*, 1305–1323.

(20) Castro, A.; Martinez, A. Intramolecular Oxidative Cyclizations in Heteroarylthioureas: A Versatile Pathway to Bridgehead Heterocyclic Systems *J. Heterocycl. Chem.* **1999**, *36*, 991–995.

(21) Vig, R.; Mao, C.; Venkatachalam, T. K.; Tuel-Ahlgren, L.; Sudbeck, E. A.; Uckun, F. M. Rational Design and Synthesis of Phenethyl-5-Bromopyridyl Thiourea Derivatives as Potent Non-Nucleoside Inhibitors of HIV Reverse Transcriptase. *Bioorg. Med. Chem.* **1998**, *6*, 1789–1797.

(22) Ashworth, R. D. B.; Crowther, A. F. Synthetic Antimalarials; Some 2-Phenylureido- and 2-Phenylthioureido-4-Dialkylaminoalkylamino-6-Methylpyrimidines. *J. Chem. Soc.* **1948**, *2*, 581—586.

(23) Nonoyama, M. Benzo[h]quinolin-10-yl-N Iridium (III) Complexes *Bull.Chem.Soc. Jpn.* **1974,** *47*, 767-768.

(24) Pelphrey, P. M.; Popov, V. M.; Joska, T. M.; Beierlein, J. M.; Bolstad, E. S. D.; Fillingham, Y. A.; Wright, D. L.; Anderson, A. C. Highly Efficient Ligands for Dihydrofolate Reductase from Cryptosporidium Hominis and Toxoplasma Gondii Inspired by Structural Analysis. *J. Med. Chem.* **2007**, *50*, 940–950.

(25) Blight, B. A.; Camara-Campos, A.; Djurdjevic, S.; Kaller, M.; Leigh, D. A.; McMillan, F. M.; McNab, H.; Slawin, A. M. Z. AAA–DDD Triple Hydrogen Bond Complexes. *J. Am. Chem. Soc.* **2009**, *131*, 14116–14122.

(26) Rowland, R. S.; Taylor, R. Intermolecular Nonbonded Contact Distances in Organic Crystal Structures: Comparison with Distances Expected from van Der Waals Radii. *J. Phys. Chem.* **1996**, *100*, 7384–7391.

(27) Hsu, C.-W.; Longhi, E.; Sinn, S.; Hawes, C. S.; Young, D. C.; Kruger, P. E.; De Cola, L. Pyrazolo[4,3-h]quinoline Ligand-Based Iridium(III) Complexes for Electrochemiluminescence. *Chem. Asian J.* **2017**, *12*, 1649–1658.

(28) We acknowledge that the Φ_{PL} value of **1•3** is ast the upper limit of the error for Φ_{PL} of **1**; the Φ_{PL} for both systems were analyzed in triplicate to verify their validity.
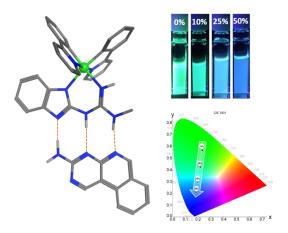
(29) We see no evidence of the lifetime component of free **3**, though this short lifetime component is likely masked by the biexponential decay and cannot be unequivocally deconvoluted from the data.

(30) Rota Martir, D.; Momblona, C.; Pertegás, A.; Cordes, D. B.; Slawin, A. M. Z.; Bolink, H. J.; Zysman-Colman, E. Chiral Iridium(III) Complexes in Light-Emitting Electrochemical Cells: Exploring the Impact of Stereochemistry on the Photophysical Properties and Device Performances. *ACS Appl. Mater. Interfaces* **2016**, *8*, 33907–33915.

(31) *Principles and Applications of Fluorescence Spectroscopy*, Jihad Rene Albani, John Wiley and Sons, **2008**.

(32) Kim, J. Il; Shin, I.-S.; Kim, H.; Lee, J.-K. Efficient Electrogenerated Chemiluminescence from Cyclometalated Iridium (III) Complexes. *J. Am. Chem. Soc.* **2005**, *127*, 1614–1615.

(33) Rota Martir, D.; Bansal, A. K.; Di Mascio, V.; Cordes, D. B.; Henwood, A. F.; Slawin, A. M. Z.; Kamer, P. C. J.; Martinez-Sarti, L.; Pertegas, A.; Bolink, H. J.; Samuel, I. D. W.; Zysman-Colman, E. Enhancing the Photoluminescence Quantum Yields of Blue-Emitting Cationic Iridium(iii) Complexes Bearing Bisphosphine Ligands. *Inorg. Chem. Front.* **2016**, *3*, 218–235.

SYNOPSIS: Presented is a demonstration of second-sphere interaction by hydrogen bonding of a heteroleptic iridium(III) complex. The triple H-bonding motif is shown to exhibit a strong enough interaction to enact a strong blue-shift in the photoluminescent spectrum, and is also observed by ^{1}H NMR, UV-Vis, CV, and computational analyses.